Electrically Conductive Composites of Polyurethane Derived From Castor Oil With Polypyrrole-Coated Peach Palm Fibers

Claudia Merlini,[1] Guilherme M.O. Barra,[1] Matthäus D.P.P. da Cunha,[1] Sílvia D.A.S. Ramôa,[1] Bluma G. Soares,[2] Alessandro Pegoretti[3]

[1]*Departamento De Engenharia Mecância, Universidade Federal De Santa Catarina, Florianópolis, Santa Catarina, Brazil*

[2]*Departamento De Engenharia Metalúrgica E De Materiais, Universidade Federal Do Rio De Janeiro, Rio De Janeiro, Rio de Janeiro, Brazil*

[3]*Department of Industrial Engineering, University of Trento, Trento 38123, Italy*

Electrically conducting fibers were prepared through *in situ* oxidative polymerization of pyrrole (Py) in the presence of peach palm fibers (PPF) using iron (III) chloride hexahydrate ($FeCl_3{\cdot}6H_2O$) as oxidant. The polypyrrole (PPy) coated PPF displayed a PPy layer on the fibers surface, which was responsible for an electrical conductivity of $(2.2 \pm 0.3) \times 10^{-1}$ S cm^{-1}, similar to the neat PPy. Electrically conductive composites were prepared by dispersing various amounts of PPy-coated PPF in a polyurethane matrix derived from castor oil. The polyurethane/PPy-coated PPF composites (PU/PPF–PPy) exhibited an electrical conductivity higher than PU/PPy blends with similar filler content. This behavior is attributed to the higher aspect ratio of PPF–PPy when compared with PPy particles, inducing a denser conductive network formation in the PU matrix. Electromagnetic interference shielding effectiveness (EMI SE) value in the X-band (8.2–12.4 GHz) found for PU/PPF–PPy composites containing 25 wt% of PPF–PPy were in the range −12 dB, which corresponds to 93.2% of attenuation, indicating that these composites are promising candidates for EMI shielding applications. POLYM. COMPOS., 38:2146–2155, 2017. © 2015 Society of Plastics Engineers

INTRODUCTION

Electrically conductive composites have been developed by addition of conductive fillers, such as intrinsically conducting polymers (ICP) and carbonaceous fillers in the insulating polymeric matrices, such as thermoplastic, thermoset polymers and unsaturated rubbers [1–4]. In the last years, considerable efforts have been made in order to develop ICP-based conductive composites with the highest electrical conductivity at low conductive filler content. These materials display an insulator-conductor transition at certain critical conductive filler content, also denoted as the percolation threshold [5, 6]. In general, weight fractions higher than 15 wt% of conducting polymer are required to reach significant increases in the electrical conductivity. However, it can lead to processing problems and also a reduction of the mechanical properties of the polymer matrix [4]. Therefore, there has been a great deal of effort spent on developing methodologies for producing conducting polymer composites with percolation threshold as low as possible in order to overcome the above mentioned limitations [5, 7, 8]. The percolation threshold and electrical conductivity are influenced by the conditions adopted for processing both matrix and conducting polymer, and the compatibility between them. Conducting polymer characteristics such as particles shape, orientation and aspect ratio can also remarkably affect the final properties of composites [5, 6]. The incorporation of conductive fillers with higher aspect ratio (width-to-thickness) in polymer matrices can be an interesting alternative to improve the electrical conductivity, once lower filler content is necessary to ensure a physical contact between them [5].

Correspondence to: C. Merlini; e-mail: dra.claudiamerlini@yahoo.com.br and Guilherme M. O. Barra; e-mail: g.barra@ufsc.br

Contract grant sponsor: Conselho Nacional de Desenvolvimento Científico e Tecnológico — CNPq; contract grant number: 400155/2014-1Contract grant sponsors: Coordenação de Aperfeiçoamento de Pessoal de Ensino Superior (CAPES) and Fundação de Amparo à Pesquisa e Inovação do Estado de Santa Catarina (FAPESC).
DOI 10.1002/pc.23790
Published online in Wiley Online Library (wileyonlinelibrary.com).

Therefore, several strategies have been used to prepare conductive additives based on ICP with higher aspect ratio and suitable to be incorporated in insulating polymer matrices. An interesting approach is the polymerization of conducting polymers on the surfaces of fibers such as amorphous silica fibers [5], insulating polymer fibers [9] and textiles fibers, for example, silk [10], polyester [11], viscose and lyocel [12], lycra [13], wool [14] and cotton [15]. Recent works have reported the production of polypyrrole (PPy) and polyaniline coated-vegetal fibers, such as banana fibers [8], coconut [7], curaua [16, 17], kenaf [18] and jute [19] by using *in situ* oxidative polymerization of pyrrole and aniline in the presence of the vegetal fibers. The use of vegetal fibers as a template for preparation of conductive fibers is encouraged since they are frequently used in composites to enhance the mechanical properties and reduce the weight and cost [16]. Additionally, they are from renewable sources and sometimes from residues generated during the transformation of natural resources into finished products [7]. Among the vegetal fibers available, peach palm fibers (PPF) (*Bactris gasipaes)* constitute an attractive alternative since they are extracted from a part of the stem that would be discarded after the extraction of the heart of palm. In this case, it is possible to reduce the amount of wastes generated and consequently, minimizing the environmental impact. Furthermore, some reports in the literature report interesting results concerning the use of polyaniline-coated-vegetal fibers as conducting filler for incorporating into insulating polymer matrices [17, 18]. Our previous works have demonstrated that ICP-coated vegetal fibers and thermosetting polyurethane (PU) derived from castor oil are interesting systems to produce conductive polymer composites with good electrical conductivity, low percolation threshold and easy of processing [7, 8]. The PU matrix selected in this work is also derived from renewable sources and displays versatile feature of molding, which allows the development of conducting composites for application in different areas, for example, in interference shielding effectiveness (EMI SE) [20–23].

Therefore, the focus of this study is on the preparation of a new material constituted of PPy-coated peach palm fibers (PPF–PPy) through *in situ* oxidative polymerization, using Iron(III) chloride hexahydrate as oxidant. The resulting PPF–PPy were incorporated in a PU matrix derived from castor oil in order to produce conductive polymer composites. The morphology, electrical conductivity and dynamic mechanical properties of PU/PPF–PPy composites were evaluated. The electromagnetic measurements of PU/PPF–PPy were also performed as a function of conductive filler content in the frequency range of 8.2–12.4 GHz in order to evaluate their potential using in shielding applications and correlate the structure and electromagnetic properties of the resulted composites [20, 21, 23].

EXPERIMENTAL

Materials

The PPF (density = 0.7 ± 0.04 g cm^{-3}) were kindly supplied by Reserva Botânica das Águas Claras from Silva Jardim city which is located in the Brazilian state of Rio de Janeiro. Pyrrole (Aldrich; 98%) was distilled under vacuum and stored in a refrigerator. Iron(III) chloride hexahydrate ($FeCl_3{\cdot}6H_2O$) (analytical grade, Aldrich Chemistry) was used without further purification. The company IMPERVEG® *Comércio e Prestações de Serviço Ltda* supplied the PU derived from castor oil (PU) (IMPERVEG® UG 132 A). The PU was provided as two components: the polyol, a trifunctional polyester, with molar mass of 928 g mol^{-1} and the prepolymer, which was synthesized by reacting diphenylmethanediisocyanate (MDI) with the castor oil polyol, remaining a percentage of the free isocyanate for subsequent reaction. Both components were mixed in the mass proportion of 2:1, respectively.

Preparation of PPy-Coated Peach Palm Fibers (PPF–PPy)

PPF were coated with PPy through *in situ* oxidative polymerization according to Merlini et al. [8]. First, 5 g of PPF with a length of 10 mm were immersed in a Becker containing 0.23 L of water. The dispersion was stirred at room temperature, and then pyrrole (0.05 mol L^{-1}) was added. After 10 min, 0.03 mol of iron(III) chloride hexahydratate ($FeCl_3{\cdot}6H_2O$) dissolved in 0.05 L of distilled water was slowly added. The polymerization was carried out using $FeCl_3{\cdot}6H_2O$/Py molar ratio of 2/1. After 6 h under magnetic stirring, the PPy-coated peach palm fibers (PPF–PPy) were washed with distilled water in order to extract the byproducts and residues of the reaction and vacuum dried at room temperature. For comparison, pure PPy was also synthesized using similar methodology.

Preparation of PU/PPF–PPy Composites

The polyol and prepolymer (mass ratio of 2/1) and PPF–PPy were blended in a reactor under vacuum for 5 min. This mixture was poured into a metallic mold, maintained for 2 h at room temperature and then subjected to compression molding at 10.7 MPa for 4 h. Composites were obtained with 5, 10, 15, 20, and 25 wt% of randomly oriented PPF–PPy, denominated as PU/PPF–PPy_*x*, where *x* represents the weight fraction of PPF–PPy in the composite. Composites with a PPF–PPy content higher than 25 wt% were not obtained due to the high viscosity of the system. Polyurethane/polypyrrole (PU/PPy) composites were also prepared following the same procedure.

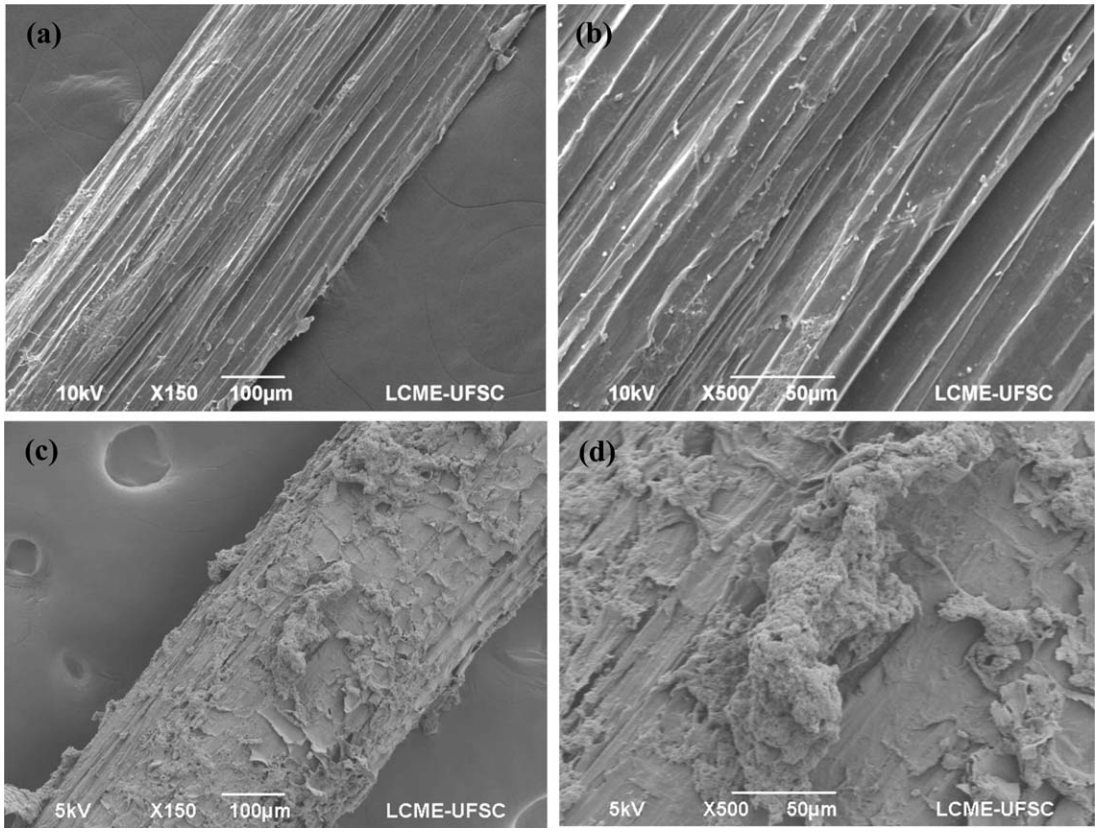

FIG. 1. SEM micrographs of PPF (a,b) uncoated and (c,d) after coating with PPy.

Characterization

Micrographs of the uncoated PPF and PU/PPF–PPy were obtained using a Jeol model JSM-6390LV scanning electron microscope (SEM). The samples were coated with gold and analyzed using an applied tension of 5–10 kV. The PU/PPF–PPy composites were previously fractured in nitrogen.

An elemental analysis (carbon, hydrogen and nitrogen) was performed with a Perkin-Elmer CHN 2400 analyzer. The combustion process was held at 925°C using pure oxygen (99.995%).

The electrical conductivity of the PPy, PPF–PPy, and low-resistivity PU/PPF–PPy and PU/PPy composites were measured using the four-probe standard method with a Keithley 6220 current source to apply the current and a Keithley Model 6517A electrometer to measure the potential difference, according to ASTM F42-93. The measurements of composites were performed on rectangular specimens with a width of 15 mm and a length of 30 mm. The PPy and PPF–PPy samples were compacted using a hydraulic press, at pressures up to 3 MPa, into cylindrical forms with 25 mm in diameter. For high-resistivity samples such as neat PU, PPF and polymer composites with low amount of PPF–PPy or PPy, the measurements were performed using a Keithley 6517A electrometer connected to a Keithley 8009 test fixture, according to ASTM D-257 methodology, on circular specimens of 90 mm of diameter. At least eight measurements were performed of each sample at room temperature (23 ± 2°C) and humidity of 50 ± 5%.

Attenuated total reflectance-Fourier transform infrared spectroscopy (ATR-FTIR) was performed on a Bruker spectrometer, model TENSOR 27, in the range of wave numbers from 4000 to 600 cm^{-1} by accumulating 32 scans at a resolution of 4 cm^{-1}.

Thermogravimetric analysis (TGA) was carried out using a STA 449 F1 Jupiter® (Netzsch) thermogravimetric analyzer. The analyses were performed at 10°C min^{-1} from 35°C to 700°C under a nitrogen flux of 25 mL min^{-1}.

The electromagnetic interference properties of PU and PU/PPF–PPy composites were measured using an Agilent Technology PNA series network analyzer (N5230C Agilent PNA-L, Santa Clara, CA) and a standard rectangular waveguide in the X-band frequency range (8.2–12.4 GHz), according reported by Schettini and Soares [23] and Schettini et al. [20]. The ε' and ε'' values were determined through scattering parameters S_{11} and S_{21} by Agilent 85071 software, in X-band frequency range (8.2 at 12.4 GHz). The electromagnetic interference shielding effectiveness (EMI SE), reflected energy (SE_R), transmitted energy (SE_T), and absorbed energy (SE_A) were

 DOI 10.1002/pc

TABLE 1. Elemental analysis, PPy content on the PPy-coated PPF and electrical conductivity.

Sample	Proportion of C	Proportion of H	Proportion of N	PPy content (wt %)[a]	Electrical conductivity (S cm^{-1})
PPF	42.3 ± 0.6	5.9 ± 0.2	0.6 ± 0.1	0.0	(3.5 ± 0.4) × 10^{-10}
PPy	54.6 ± 0.1	3.9 ± 0.1	15.7 ± 0.1	100.0	1.5 ± 0.2
PPF–PPy	46.8 ± 0.7	5.6 ± 0.2	6.3 ± 0.1	36.3± 0.2	(2.2 ± 0.3) × 10^{-1}

[a]From CHN elemental analysis.

calculated from complex scattering parameters that correspond to reflection (S^*_{11}) and transmission (S^*_{21}). Electromagnetic properties measurements were performed on rectangular specimens with a width of 10 mm, a length of 23 mm and a thickness of 2.0 mm.

The dynamic mechanical properties of the composites and PU were studied using a dynamic mechanical analyzer (DMA-983 interfaced to a TA 2000). The DMA measurements were carried out in a nitrogen gas environment, at a heating rate of 5°C min^{-1} and at 1 Hz with a single cantilever.

RESULTS AND DISCUSSION

Characterization of PPy-Coated Peach Palm Fibers (PPF–PPy)

SEM micrographs of the uncoated and PPy-coated PPF surfaces are shown in Fig. 1. PPF displays a rough and corrugated surface and bundles of microfibrils can be seen (Fig. 1a and b). Moreover, the SEM micrographs of the PPF–PPy show a continuous and compact PPy layer homogeneously coating the PPF surface. The presence of some PPy agglomerates can also be observed.

Table 1 shows the elemental analysis of CHN, PPy content and electrical conductivity of neat PPy, uncoated and coated PPF. The PPy content on the fiber surface was calculated from the proportion of nitrogen in the PPy-coated PPF and neat PPy, according to the procedure described in the literature [17]. The PPy amount in the PPF fibers surface was of 36.3 wt%. It is worthwhile to observe that the conductive layer on the PPF surface is responsible for the high electrical conductivity of (2.2 ± 0.3) × 10^{-1} S cm^{-1}, which is close to that of neat PPy (1.5 ± 0.1 S cm^{-1}) and about 9 orders of magnitude higher than those of neat PPF ((3.5 ± 0.2) × 10^{-10} S cm^{-1}).

Figure 2 shows the FTIR spectra of the PPF, PPy and PPF–PPy. The spectrum of PPF exhibits an absorption band at 3335 cm^{-1}assigned to stretching vibrations of the hydroxyl group [16]. The bands at 2974 and 2905 cm^{-1} are related to the stretching of the methyl and methylene groups, respectively [8]. The C═O stretching vibrations of the hemicellulose and lignin are represented by the bands at 1734 and 1647 cm^{-1}, respectively [7, 24]. The bands at 1377, 1242, and 1038 cm^{-1} can be ascribed to the C—H asymmetric deformation, C—O stretching vibration of the acetyl group of hemicellulose and to plane deformation of the aromatic C—H, respectively. At 1157 cm^{-1} a band related to C—O—C groups can be observed [25]. The PPy spectrum displays absorption bands at 1533 and 1448 cm^{-1} assigned to the C—C and C—N stretching vibration of Py ring [26, 27]. Moreover, the band at 1286 cm^{-1}is ascribed to the C—H or C—N in-plane deformation [28, 29] and the bands at 1157 and 1032 cm^{-1} are related to the C—H bending modes [27]. The PPy-coated PPF spectrum shows the predominance of PPy absorption bands, evidencing that the PPy is deposited on the PPF fibers surface forming an external layer, as observed in the SEM micrographs.

Mass loss curves obtained by TGA and the first derivative (DTG) for PPF, PPF–PPy and PPy are shown in Fig. 3. PPy exhibits a continuous weight loss starting at 200°C that is assigned to the polymer chain degradation. The PPF curve shows three weight loss stages, with the first one occurring below 100°C due to the water elimination. The second stage at 284°C corresponds to the depolymerization of hemicelluloses and the cleavage of glycosidic linkages of cellulose and, the third one at 334°C is related to the decomposition of α-cellulose. The decomposition of the lignin occurs in a broad range of temperature between 200 and 400°C and probably it is overlapped with the hemicellulose and α-cellulose decomposition [30, 31]. The TGA curve of the PPy-coated PPF displays similar behavior to that observed for the neat PPF. However, PPF–PPy shows lower onset degradation

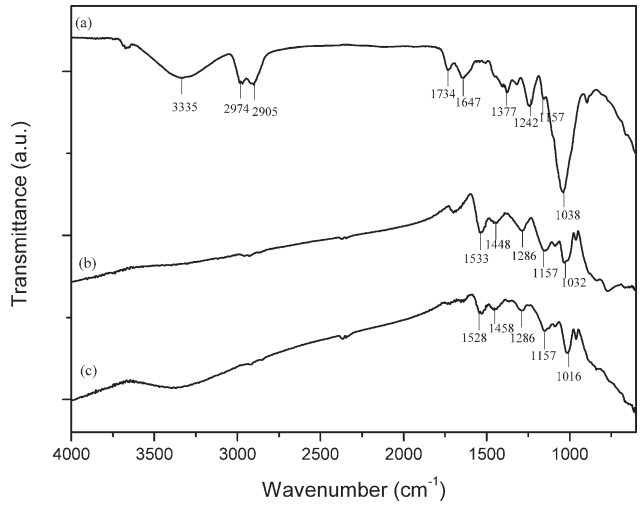

FIG. 2. FTIR spectra of (a) uncoated PPF, (b) PPy, and (c) PPF–PPy.

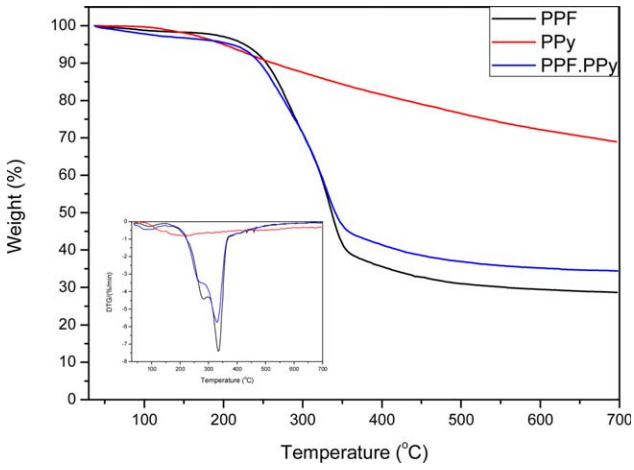

FIG. 3. TGA and DTG curves for uncoated PPF, PPy and PPF–PPy. [Color figure can be viewed at wileyonlinelibrary.com.]

temperatures that can be attributed to the external PPy layer, which has a lower degradation temperature.

Characterization of PU/PPF–PPy Composites

The PPy-coated PPF were used as conductive filler for incorporating into PU derived from castor oil. Figure 4 shows the FTIR spectra of the PU and of PU/PPF–PPy composites with different weight fractions of PPF–PPy. The spectrum of PU exhibits absorption bands at 3,338; 2,924; and 2,855 cm^{-1} related to the deformations of the N—H, C—H_3 and C—H_2, respectively. The absorption band at 2,276 cm^{-1} can be attributed to the free isocyanate groups, indicating that there is an excess of NCO— group in the polymer backbone. The absorption bands due to the carbonyl stretching vibration of the urethane pre-polymer and C—C occur at 1,726 and 1,599 cm^{-1}, respectively. The absorption band at 1,524 cm^{-1} is associated to the combination of C—N stretching vibration and N—H deformation. The absorption bands at 1,219 and 1,045 cm^{-1} are attributed to the ether groups [25, 32]. The FTIR spectra of PU/PPF–PPy composites show absorption bands similar to those of neat PU, however, the absorption band at 2,276 cm^{-1} is not observed, indicating the disappearance of the free NCO group. This behavior suggests that the free isocyanate groups in the PU matrix were able to react and produce crosslink with the —N—H group of the PPy on the surface of the PPF.

Figure 5 illustrates the SEM micrographs of cryogenically fractured surfaces of the PU/PPF–PPy composites containing 5, 15, and 25 wt% of PPF–PPy. Micrographs show that PPF–PPy are dispersed in the PU matrix and, as expected, with increasing the filler content higher amount of PPy-coated fibers per area can be detected, inducing a denser conducting network formation. Composites fracture surfaces showed apparently good interfacial adhesion of both components and, there is no evidence of voids. It is possible to note the presence of fibers break and limited fibers pull out, suggesting a good level of fiber/matrix adhesion.

The curves of storage modulus (E') as a function of temperature for PU and PU/PPF-PPy composites are reported in Fig. 6a. As the temperature increases from −20°C the storage modulus changes from the glassy to the rubery state crossing the glass transition temperature (T_g) of the PU matrix [32, 33]. As expected, the storage modulus of neat PU is lower than that of composites especially in the rubbery region, suggesting that the incorporation of PPF–PPy enhances the stiffness of the material. Moreover, PU/PPF–PPy composites exhibit a slightly increase in the storage modulus as the conductive filler content increases. According to Manoharan, et al. [33], E' is influenced by the interfacial bonding between fiber and matrix, which induces an effective stress transfer and, hence the mobility of the matrix polymer chains is reduced.

Loss tangent (tan δ) thermograms for PU and PU/PPF–PPy composites are reported in Fig. 6b. The tan δ_{max} peak of PU was observed at 32°C, which corresponds to the T_g of PU matrix [32]. For PU/PPF–PPy composites, the T_g remains almost the same as the conductive filler content increases. Moreover, with increasing conductive filler loading the tan δ intensity is reduced significantly due to the presence of the fibers that restrict the PU chains mobility.

By taking the amount of PPy incorporated on fibers surface of 36.3 wt% into consideration (as determined by CHN elemental analysis,), the amount of PPy in the PU/PPF–PPy composites was estimated. Therefore, the PPy content in the composites containing 5, 10, 15, 20 and 25 wt% of PPF–PPy was 1.8, 3.6, 5.4, 7.3, and 9.1 wt%, respectively. Composites containing neat PPy were also prepared in order to compare the electrical conductivity values with those composites containing PPy-coated PPF. The electrical conductivity as a function of PPy content

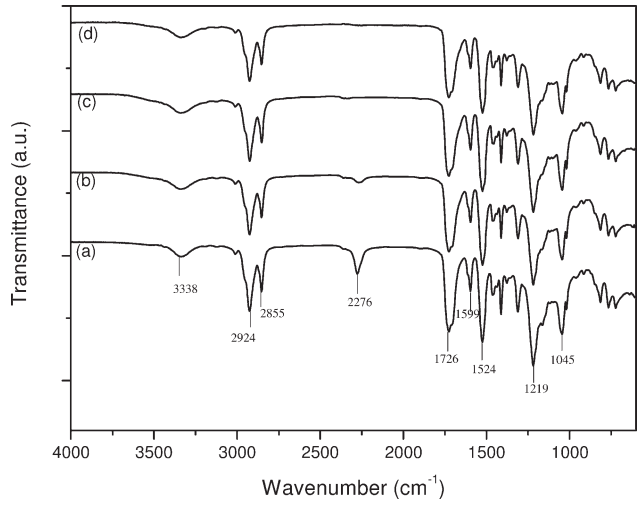

FIG. 4. FTIR spectra of: (a) PU and PU/PPF–PPy composites containing (b) 5 wt%, (c) 15 wt%, and (d) 25 wt% of PPF–PPy.

DOI 10.1002/pc

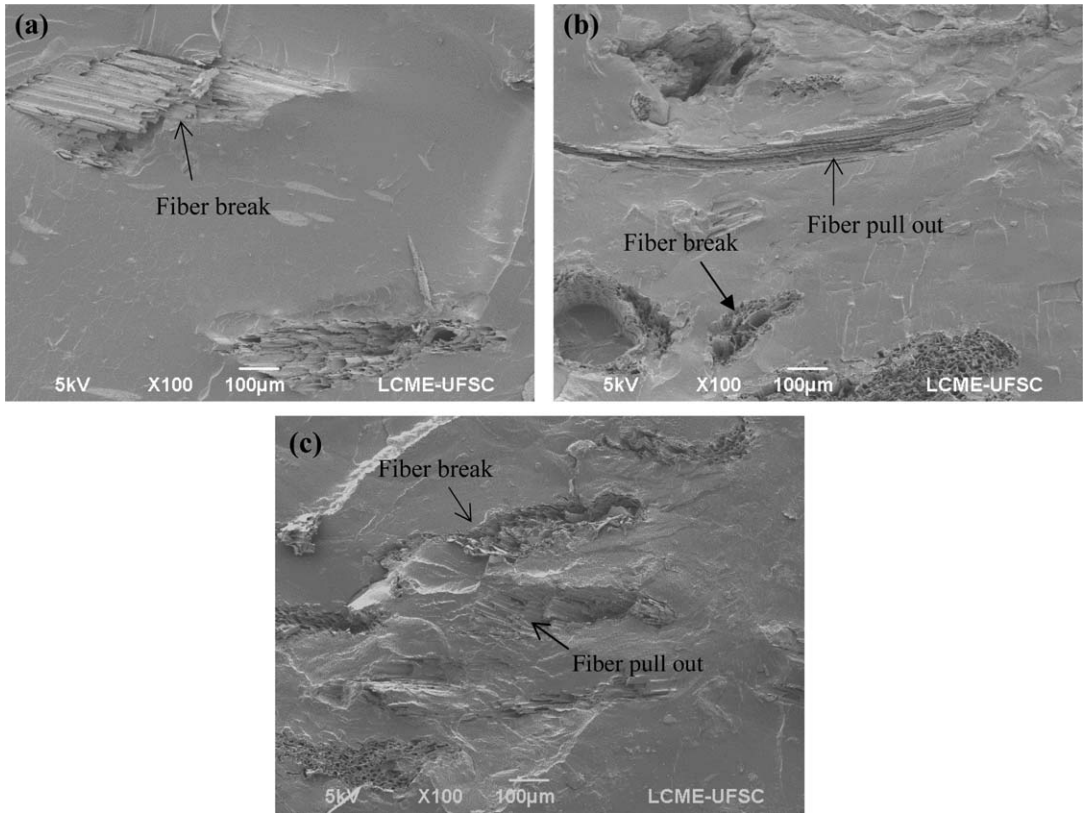

FIG. 5. Scanning electron micrographs of the PU/PPF–PPy composites with PPF–PPy content of: (a) 5 wt%, (b) 15 wt%, and (c) 25 wt%.

on the PU/PPF–PPy and PU/PPy composites is reported in Fig. 7a. With increasing the PPy content in both composites, the electrical conductivity increases significantly due to the formation of a conducting pathway in the PU matrix. PU/PPF–PPy composites present higher electrical conductivity at lower PPy content than those found for PU/PPy composites. This behavior can be associated to the fillers geometry, in which the PPy-coated PPF display higher aspect ratio when compared with the neat PPy. The microstructure of the PU/PPF–PPy composite indicates that the geometry modification of the conductive filler was able to improve the formation of the conducting network in the PU matrix and, consequently, to increase the electrical conductivity.

The data presented in Fig. 7a were fitted to the scaling law of percolation theory [34], as observed in *Eq. 1*; in which c is a constant, t a critical exponent, σ_f the conductivity, f the fraction of the conductive filler and f_p the fraction at the percolation threshold, expressed as a weight fraction.

$$\sigma_f = c\left(f - f_p\right)^t \tag{1}$$

The experimental data were used to plot the variation of σ_f as a function of log $(f - f_p)$ (Fig. 7b) from which it is possible to estimate the percolation threshold of the system [5, 35]. The percolation threshold (f_p) were 2.5 and 1.8 wt% for composites containing PPy and PPF–PPy, respectively, calculated with a linear correlation coefficient (R) of ~0.99. It is interesting to note that the percolation threshold of PU/PPF–PPy is lower than that of PU/PPy composites, probably due to the high aspect ratio of PPy-coated PPF fibers dispersed in the PU matrix. This result corroborates those reported in the literature, in which a lower percolation threshold was also observed for polymer systems containing disperse phase of polyaniline-coated coconut fibers [7], PPy-coated amorphous silica fibers [5] and PPy-coated polyamide 66 or PP fibers [9] when compared to the same insulating polymer matrix with spherical particles of the conducting phase.

The critical exponent (t) values calculated from the plot of log σ versus log $(f - f_p)$ were 5.0 and 13.8 for PU/PPy and PU/PPF–PPy composites, respectively. The value of the critical exponent for PU/PPy composites was quite similar to that reported for SEBS/PPy systems [5]. According to Grimaldi et al. [34], this behavior could be attributed to a tunneling mechanism. On the other hand, the t value for PU/PPF–PPy composite was higher than PU/PPy composites, probably because of the higher aspect ratio of fibers, as reported by Al-Saleh and Sundararaj [36].

The electromagnetic interference shielding effectiveness (EMI SE) of a material can be defined as the ratio between

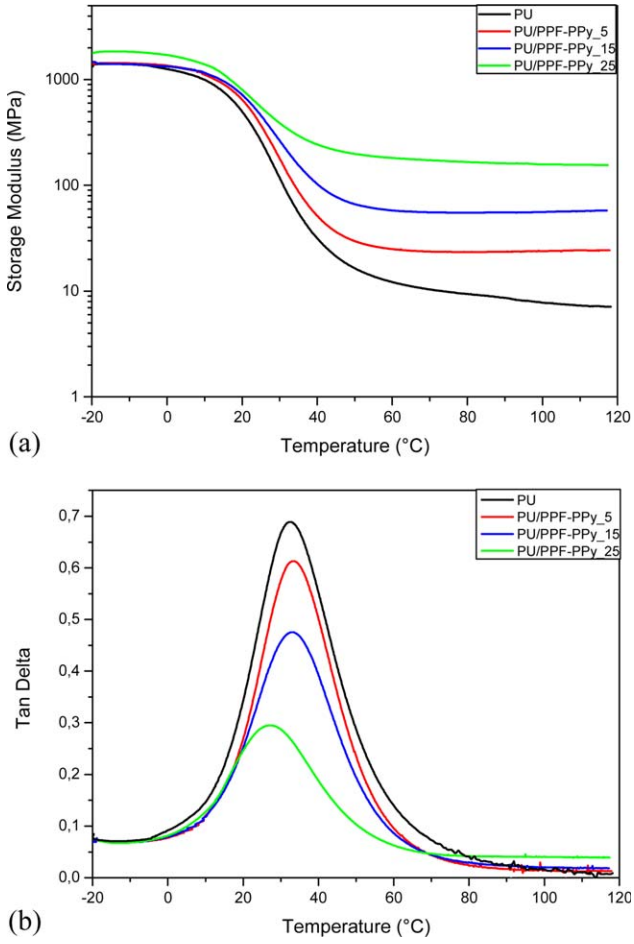

FIG. 6. DMTA traces (a) storage modulus and (b) loss factor of PU/PPF–PPy composites with various fillers contents. [Color figure can be viewed at wileyonlinelibrary.com.]

incident (I) to transmitted (T) power. Hence, for EMI SE measured in decibels (dB) it is given by *Eq. 2* [6, 37]:

$$\text{EMISE (dB)} = 10\log\frac{I}{T} \tag{2}$$

Figure 8 shows the EMI SE of the pure PU, PU/PPF–PPy composites as a function of conductive filler content in the frequency range from 8 to 12.4 GHz. The EMI SE of PU/PPF–PPy composites increase with increasing the PPF–PPy content, due to the formation of a conducting pathways into PU matrix [38]. Composites containing 25 wt% of PPF–PPy displays an electromagnetic attenuation of −12.0 dB over all frequency ranges studied which corresponds to 93.2% of attenuation. Furthermore, the shielding effectiveness is slightly influenced for the frequencies lower than 9 GHz.

Figure 9 shows the dependence of EMI SE as a function of PPy coated fibers content for frequencies at 8.2, 10 and 12.4 GHz. It is also present in the Fig. 9 the linear regression models of the EMI SE and conductive filler content for each frequency at 8.2, 10 and 12.4 GHz. This linear regression model can be used for prediction the PPF–PPy amount (X) for a desired EMI SE value, at a specific frequency, or to estimate EMI SE for a composite with a PPF–PPy amount [22]. With increasing the conductive filler content the shielding efficiency for all composites enhanced linearly. As mentioned on the above the EMI SE of composites is independent for frequency higher than 9 GHz. On the other hand, for 8.2 GHz, the EMI SE is slightly lower than those found for 10 and 12.4 GHz.

The amount of attenuation of a conductive composite depends on different mechanisms: reflection (SE_R), absorption (SE_A) and multiple reflection (SE_M) [6, 39]. The incident (I), transmitted (T) and reflected (R) power data were collected directly by the instrument used to measure the EMI SE of the sample, in order to evaluate the contribution of reflection and absorption to the total EMI SE of the composites [6]. The complex scattering parameters that represent the reflection S_{11} (S_{22}) and transmission S_{12} (S_{21}) coefficients were compared with the incident electromagnetic wave, according to the following equations:

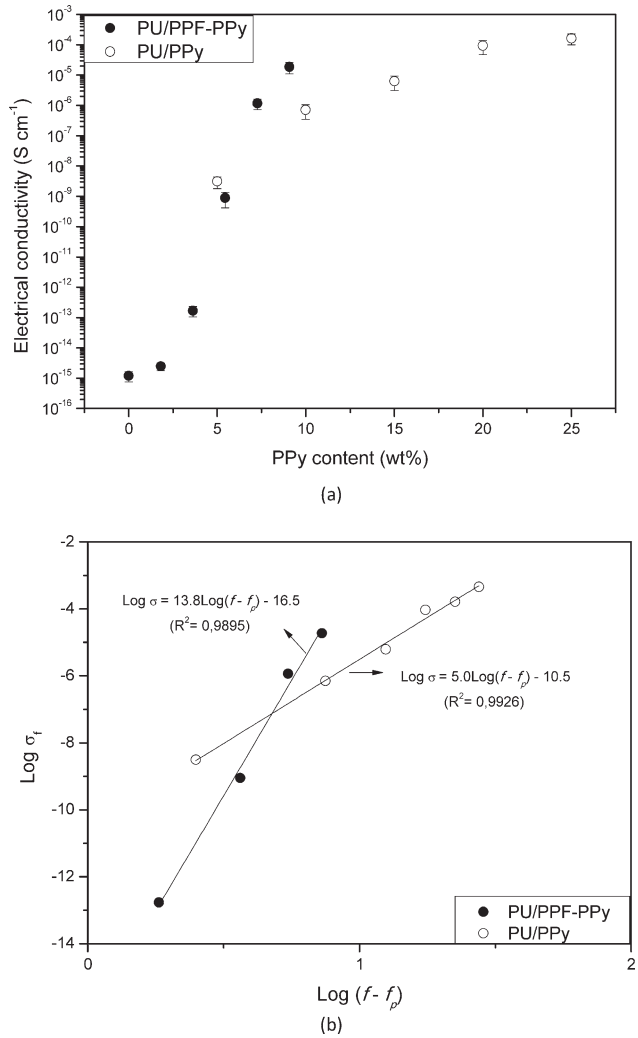

FIG. 7. Plot of (a) Electrical conductivity as a function of PPy content (by weight) in the composites PU/PPF–PPy and PU/PPy and (b) log σ_f as a function of log $(f - f_p)$.

DOI 10.1002/pc

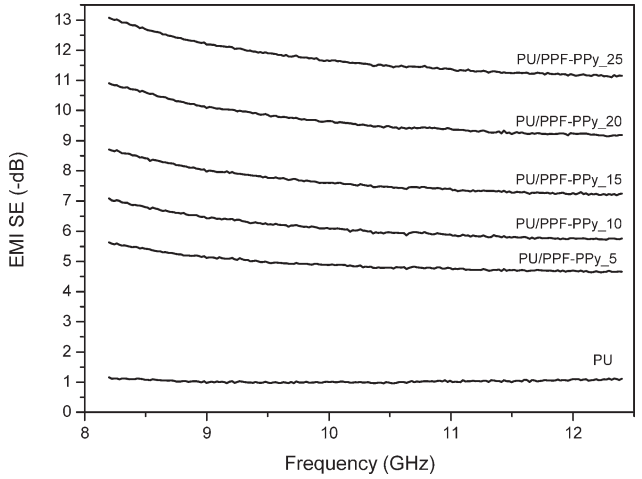

FIG. 8. EMI SE of PU/PPF–PPy composites with various fillers contents.

$$T=\left|\frac{E_T}{E_I}\right|^2=|S_{12}|^2\left(=|S_{21}|^2\right) \tag{3}$$

$$R=\left|\frac{E_R}{E_I}\right|^2=|S_{11}|^2\left(=|S_{22}|^2\right) \tag{4}$$

The absorption power (A) is then determined by:

$$A=1-R-\mathrm{T} \tag{5}$$

where R is the reflection power obtaining from the S_{11} (S_{22}) scattering parameter, and T is the transmission power obtaining from the S_{21} (S_{12}) scattering parameter [38, 40].

The contribution of SE_A (dB) and SE_R to the EMI SE of PU and composites was determined using the experimental power data and *Eqs*. 6–8:

$$\mathrm{SE}_R=10\log\frac{I}{I-R} \tag{6}$$

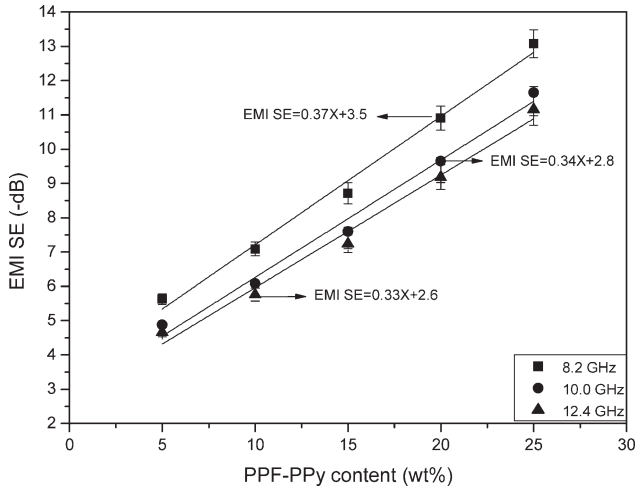

FIG. 9. EMI SE as a function of PPF–PPy content.

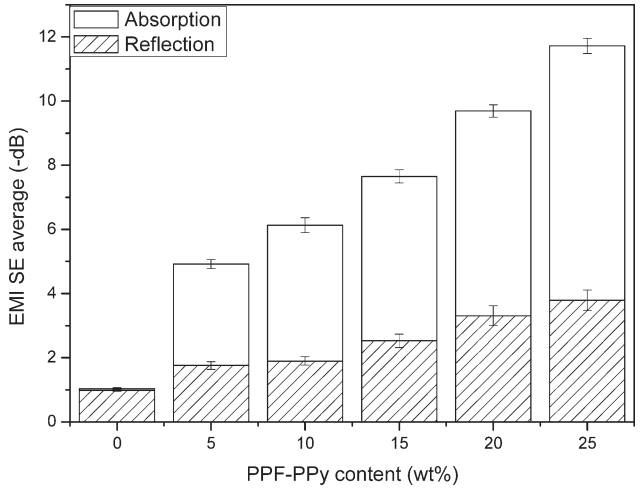

FIG. 10. Influence of absorption and reflection mechanisms on the EMI SE of the PU/PPF–PPy composites with various fillers contents.

$$SE_A=10\log\frac{I-R}{T} \tag{7}$$

$$\begin{aligned}\text{EMI SE}&=SE_A+SE_R=10\log\frac{I}{I-R}\\&+10\log\frac{I-R}{T}=10\log\frac{I}{T}\end{aligned} \tag{8}$$

To understand the influence of each shielding mechanism on the overall EMI SE of the composites, the contribution of reflection and absorption in the total EMI SE is reported in Fig. 10. The data are reported as average values in the range frequency of 8.2–12.4 GHz. The shielding by reflection and absorption of PU/PPF–PPy composites increases with PPF–PPy loading, resulting in higher EMI SE. However, the shielding by absorption is higher than that by reflection.

Figure 11 shows the real (ε') and the imaginary part (ε'') of the complex permittivity spectra of the PU/PPF–PPy composites. The real part (ε') of the complex permittivity can be mainly associated with the polarization occurring at the interface between the matrix and the conducting polymer, and the imaginary part (ε'') is related to the dissipation of energy from free electrons [38, 40]. For PU/PPF–PPy composites, both the real and imaginary permittivity increase as the concentration of PPF–PPy increases. The increase of real and imaginary part of the permittivity can be attributed to the interfacial polarization [41]. Moreover, at low weight fractions of PPF–PPy, the real and imaginary part of the permittivity are almost independent on the frequencies. However, at higher loading, the values decrease with increasing of frequency. According to Varshney et al. [42] the real and imaginary part of the permittivity decreases with increasing the frequency due to the difficult of the dipoles to reorient themselves fast enough when electric field is applied. Therefore, with increasing the frequency the interfacial polarizations decreases, and hence, the loss factor (ε'') is reduced. Moreover, with increasing PPF–PPy content ε''

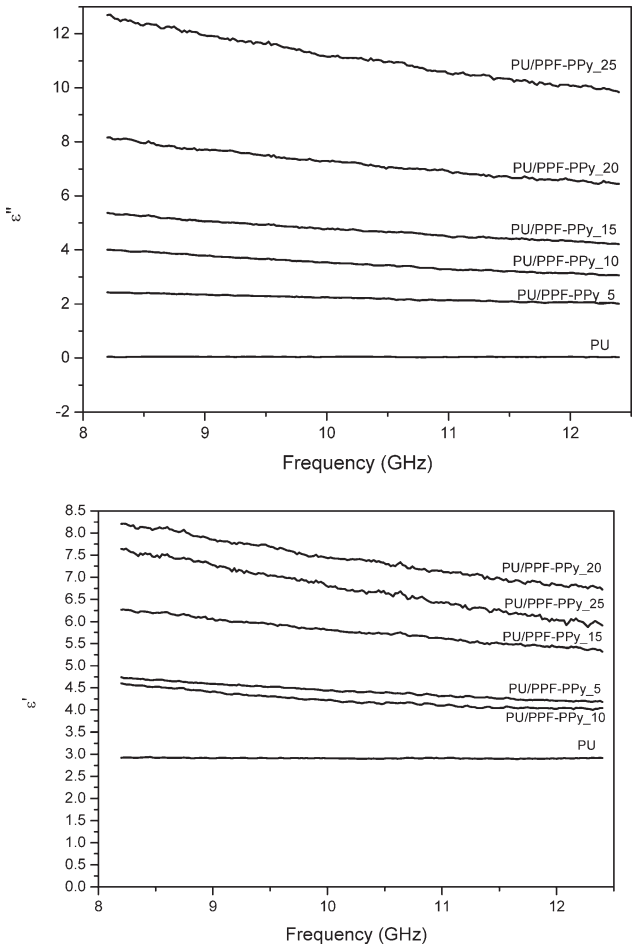

FIG. 11. Dependence of the real (ε') and the imaginary part (ε'') of the complex permittivity on the frequency of PU/PPF–PPy composites.

becomes higher than ε', resulting in high values of tan δ ($\varepsilon''/\varepsilon'$) and a better absorption behavior (SE_A) can be observed [43], as shown in Fig. 10. The dielectric results are in agreement with the electrical conductivity and EMI SE measurements of the composites.

CONCLUSIONS

Conducting PPF coated with PPy were successfully prepared through *in situ* oxidative chemical polymerization of pyrrole. SEM micrographs and FTIR spectroscopy revealed that the PPF were completely coated with an uniform PPy layer which lead to a substantial increase of the electrical conductivity to values of $(2.2 \pm 0.3) \times 10^{-1}$, similar to that of neat PPy. The amount of PPy deposited on fiber surface, as determined by CHN elemental analysis, was about 36.3 wt%. Electrically conductive composites prepared by adding various amounts of PPy-coated PPF in PU derived from castor oil display good interfacial adhesion and the absence of bands related to free isocyanate groups, suggesting some interaction degree between PPF–PPy and matrix. The incorporation of PPF–PPy affects stiffness of the material and the storage modulus slightly increase as the conductive filler content increases. It was demonstrated that lower PPF–PPy content incorporated in the PU matrix is necessary to reach higher electrical conductivity than that polymer system containing PPy spherical particles. These results indicate that by increasing the aspect ratio of conductive filler the percolation threshold can be decreased, i.e., lower filler concentration is required to achieve a conductive path when compared with addition of PPy. PU/PPF–PPy composites also presented good electromagnetic interference shielding effectiveness, with a shielding mechanism mainly based on absorption. These results are encouraging for a possible application of the PPy-coated PPF as conductive additive in a PU matrix with EMI shielding applications.

ACKNOWLEDGMENT

The authors sincerely thank the Laboratório Central de Microscopia Eletrônica, Federal University of Santa Catarina (LCME-UFSC).

NOMENCLATURE

ATR	Attenuated total reflectance
FTIR	Fourier transform infrared spectroscopy
ICP	Intrinsically conducting polymers
MDI	Diphenylmethanediisocyanate
PPF	Peach palm fiber
PPy	Polypyrrole
PU	Polyurethane
TGA	Thermogravimetric analysis

REFERENCES

1. A. Job, F. Oliveira, N. Alves, J. Giacometti, and L. Mattoso, *Synth. Met*., **135**, 99 (2003).
2. C. Merlini, G.M. de Oliveira Barra, T.M. Araujo, and A. Pegoretti, *Synth. Met*., **196**, 186 (2014).
3. M.E. Leyva, G.M.O. Barra, M.M. Gorelova, B.G. Soares, and M. Sens, *J. Appl. Polym. Sci*., **80**, 626 (2001).
4. G.M.O. Barra, M.E. Leyva, B.G. Soares, L.H. Mattoso, and M. Sens, *J. Appl. Polym. Sci*., **82**, 114 (2001).
5. C. Merlini, B.S. Rosa, D. Müller, L.G. Ecco, S.D.A.S. Ramôa, and G.M.O. Barra, *Polym. Test*., **31**, 971 (2012).
6. S.D.A.S. Ramôa, G.M.O. Barra, R.V.B. Oliveira, M.G. de Oliveira, M. Cossa, and B.G. Soares, *Polym. Int*., **62**, 1477 (2013).
7. C. Merlini, G.M.O. Barra, D.P. Schmitz, S.D.A.S. Ramoa, A. Silveira, T.M. Araujo, and A. Pegoretti, *Polym. Test*., **38**, 18 (2014).
8. C. Merlini, S.D.A.S. Ramoa, and G.M.O. Barra, *Polym. Compos*., **34**, 537 (2013).
9. X.H. Yin, K. Kobayashi, K. Yoshino, H. Yamamoto, T. Watanuki, and I. Isa, *Synth. Met*., **69**, 367 (1995).
10. I. Cucchi, A. Boschi, C. Arosio, F. Bertini, G. Freddi, and M. Catellani, *Synth. Met*., **159**, 246 (2009).
11. J. Molina, A.I. del Río, J. Bonastre, and F. Cases, *Eur. Polym. J*., **44**, 2087 (2008).

12. L. Dall'Acqua, C. Tonin, A. Varesano, M. Canetti, W. Porzio, and M. Catellani, *Synth. Met*., **156**, 379 (2006).
13. J. Wu, D. Zhou, C.O. Too, and G.G. Wallace, *Synth. Met*., **155**, 698 (2005).
14. A. Varesano and C. Tonin, *Text. Res. J*, **78**, 1110 (2008).
15. A. Kaynak, S.S. Najar, and R.C. Foitzik, *Synth. Met*., **158**, 1 (2008).
16. F.G. Souza, G.E. Oliveira, C.H.M. Rodrigues, B.G. Soares, M. Nele, and J.C. Pinto, *Macromol. Mater. Eng*., **294**, 484 (2009).
17. J.R. Araujo, C.B. Adamo, and M.A. De Paoli, *Chem. Eng. J*., **174**, 425 (2011).
18. S.I.A. Razak, W.A.W.A. Rahman, N.F.A. Sharif, N.H.M. Nayan, M.A.A. Saidi, and M.Y. Yahya, *Comp. Interf*., **20**, 611 (2013).
19. P.A. Kumar, S. Chakraborty, and M. Ray, *Chem. Eng. J*., **141**, 130 (2008).
20. A.R.A. Schettini, D. Khastgir, and B.G. Soares, *Polym. Eng. Sci*., **52**, 2041 (2012).
21. M. Magioli, B.G. Soares, A.S. Sirqueira, M. Rahaman, and D. Khastgir, *J. Appl. Polym. Sci*., **125**, 1476 (2012).
22. V. Šafářová and J. Militký, *Polym. Compos*., 1 (2015).
23. A.R.A. Schettini and B.G. Soares, *Macromol. Symp*., **299300**, 164 (2011).
24. E.N. Pires, C. Merlini, H.A. Al-Qureshi, G.V. Salmória, and G.M.O. Barra, *Polymer*, **22**, 339 (2012).
25. E. Sinha, and S.K. Rout, *J. Mater. Sci*., **43**, 2590 (2008).
26. S.D.A.dS. Ramôa, C. Merlini, G.M.dO. Barra, and B.G. Soares, *Polymer*, **24**, 57 (2014).
27. N.V. Blinova, J. Stejskal, M. Trchová, J. Prokeš, and M. Omastová, *Eur. Polym. J*, **43**, 2331 (2007).
28. M. Omastová, M. Trchová, J. Kovářová, and J. Stejskal, *Synth. Met*., **138**, 447 (2003).
29. C. Merlini, R. d. S. Almeida, M.A. D'Ávila, W.H. Schreiner, and G.M. d. O. Barra, *Mater. Sci. Eng. B*, **179**, 52 (2014).
30. A.S. Santos, M.Z. Farina, A.P. Pezzin, and D.A.K. Silva, *J. Reinf. Plast. Compos.* **27**, 1805, (2008).
31. L.B. Manfredi, E.S. Rodríguez, M. Wladyka-Przybylak, and A. Vázquez, *Polym. Degrad. Stab*., **91**, 255 (2006).
32. C. Merlini, V. Soldi, and G.M.O. Barra, *Polym. Test*., **30**, 833 (2011).
33. S. Manoharan, B. Suresha, G. Ramadoss, and B. Bharath, *J. Mater. Sci*., **2014**, (2014).
34. C. Grimaldi, T. Maeder, P. Ryser, and S. Strässler, *J. Phys. D Appl. Phys.* **36**, 1341 (2003).
35. M.E. Leyva, G.M.O. Barra, and B.G. Soares, *Synth. Met*., **123**, 443 (2001).
36. M.H. Al-Saleh and U. Sundararaj, *Compos. Part A: Appl. Sci. Manuf*., **39**, 284 (2008).
37. N.F. Colaneri and L.W. Schacklette, *IEEE Trans. Instrum. Meas*, **41**, 291 (1992).
38. J. Marins, B. Soares, M. Fraga, D. Müller, and G.O. Barra, *Cellu*, **21**, 1409 (2014).
39. Y. Wang and X. Jing, *Polym. Adv. Technol*., **16**, 344 (2005).
40. S. Dhawan, K. Singh, A. Bakhshi, and A. Ohlan, *Synth. Met*., **159**, 2259 (2009).
41. J. Azadmanjiri, P. Hojati-Talemi, G.P. Simon, K. Suzuki, and C. Selomulya, *Polym. Eng. Sci*., **51**, 247 (2011).
42. S. Varshney, A. Ohlan, V.K. Jain, V.P. Dutta, and S.K. Dhawan, *Mater. Chem. Phys*., **143**, 806 (2014).
43. A. Gupta and V. Choudhary, *Comp. Sci. Technol*., **71**, 1563 (2011).